ISSN 0016-7037
Volume 86
June 1, 2012

ELSEVIER

Geochimica et Cosmochimica Acta

JOURNAL OF THE GEOCHEMICAL SOCIETY
AND THE METEORITICAL SOCIETY

Continued on outside back cover

Available online at www.sciencedirect.com

SciVerse ScienceDirect

Geochimica et Cosmochimica Acta 86 (2012) 21–36

Geochimica et Cosmochimica Acta

www.elsevier.com/locate/gca

Neon diffusion kinetics in olivine, pyroxene and feldspar: Retentivity of cosmogenic and nucleogenic neon

Loraine Gourbet [a,b], David L. Shuster [b,c,*], Greg Balco [b], William S. Cassata [c,b], Paul R. Renne [b,c], Dylan Rood [d,1]

[a] Department of Earth Science, Ecole normale supérieure de Lyon, France
[b] Berkeley Geochronology Center, 2455 Ridge Road, Berkeley, CA 94709, USA
[c] Department of Earth and Planetary Science, University of California, Berkeley, CA 94720, USA
[d] Center for Accelerator Mass Spectrometry, Lawrence Livermore National Laboratory, Livermore, CA 94550, USA

Received 26 October 2011; accepted in revised form 3 March 2012; available online 13 March 2012

Abstract

We performed stepwise degassing experiments by heating single crystals of neutron- or proton-irradiated olivine, pyroxene and feldspar to study diffusion kinetics of neon. This is important in evaluating the utility of these minerals for cosmogenic ^{21}Ne measurements and, potentially, for Ne thermochronometry. Degassing patterns are only partially explained by simple Arrhenius relationships; most samples do not exhibit a precisely-determined activation energy in an individual diffusion domain. Regardless, we find clear differences in diffusion kinetics among these minerals. Based on sub-selected data, our estimates for neon diffusion kinetics (activation energy E_a and pre-exponential factor D_o, assuming the analyzed fragments approximate the diffusion domain) in each mineral are as follows: for the feldspars, E_a ranges from ~65 to 115 kJ/mol and D_o from 3.9×10^{-3} to 7.1×10^{2} cm^{2}s^{-1}; for the pyroxenes, E_a ranges from ~292 to 480 kJ/mol and D_o from 1.6×10^{2} to 2.9×10^{11} cm^{2}s^{-1}; for the olivines, E_a ranges from ~360 to 370 kJ/mol and D_o from 1.5×10^{6} to 5.0×10^{6} cm^{2}s^{-1}. Differences in these parameters are broadly consistent with the expected effect of structural differences between feldspar, and olivine and pyroxene. These results indicate that cosmogenic ^{21}Ne will be quantitatively retained within olivine and pyroxene at Earth surface temperatures over geological timescales. The diffusion kinetics for feldspars, on the other hand, predicts that ^{21}Ne retention at Earth surface temperatures will vary significantly with domain size, crystal microtexture, surface temperature, and exposure duration. Quantitative retention is expected only in favorable conditions. This conclusion is reinforced by additional measurements of cosmogenic ^{21}Ne in coexisting quartz and feldspar from naturally irradiated surface samples; sanidine from a variety of rhyolitic ignimbrites exhibits quantitative retention, whereas alkali–feldspar from several granites does not.

1. INTRODUCTION

Observations of neon (Ne) isotopes in minerals have broad utility in the Earth and planetary sciences, including applications to cosmochemistry, mantle geochemistry, thermochronometry, and geomorphology. The stable isotopes of Ne are ^{20}Ne (90.48% of the atmospheric neon), ^{21}Ne (0.27%), and ^{22}Ne (9.25%); the atmospheric concentration of Ne is 18.2 ppm (Eberhardt et al., 1965; Porcelli et al., 2002). In minerals, Ne is produced in situ by nuclear reactions with cosmic rays (cosmogenic neon) and alpha particles from the U–Th radioactive decay chains (nucleogenic neon).

Cosmogenic ^{21}Ne is primarily produced in surface rocks exposed to the cosmic-ray flux by spallation reactions induced by high-energy neutrons, and secondarily by muon

* Corresponding author at: Department of Earth and Planetary Science, University of California, Berkeley, CA 94720, USA.
E-mail address: dshuster@berkeley.edu (D.L. Shuster).
[1] Present address: AMS Laboratory, Scottish Universities Environmental Research Centre, East Kilbride G75 0QF, UK.

0016-7037/$ - see front matter © 2012 Elsevier Ltd. All rights reserved.
http://dx.doi.org/10.1016/j.gca.2012.03.002

interactions (Fernandez-Mosquera et al., 2010). Like other cosmic-ray-produced nuclides, ^{21}Ne is commonly used to quantify terrestrial surface exposure ages and erosion rates, as well as exposure ages of meteorites (Phillips et al., 1998; Niedermann, 2002; Kober et al., 2007 and references therein). A prerequisite for these applications is that, once it is produced, ^{21}Ne is quantitatively retained at the production site until the time of measurement. However, depending on the kinetics of noble gas diffusion within a particular mineral, significant loss of cosmic-ray-produced noble gases may occur even at temperatures as low as 20 °C (e.g., ^{3}He in quartz; Shuster and Farley, 2005). Knowledge of neon diffusion kinetics is therefore required for quantitative interpretation of cosmogenic Ne observations.

To date, most terrestrial applications of cosmogenic ^{21}Ne have been restricted to quartz, with fewer studies involving pyroxene (e.g., Bruno et al., 1997; Schäfer et al., 1999), olivine (e.g., Fenton et al., 2009) and feldspar (e.g., Kober et al., 2005). Several studies have quantified ^{21}Ne production rates in quartz (Niedermann, 2002; Balco and Shuster, 2009; Amidon et al., 2009; Goethals et al., 2009; Kober et al., 2011), and quantitative retention of ^{21}Ne in quartz at Earth surface temperatures has been clearly established by both laboratory diffusion experiments and observations of natural samples (Niedermann et al., 1994; Kober et al., 2005; Shuster and Farley, 2005). It is probably safe to assume that minerals that tightly retain He (e.g., olivine and pyroxene; Trull et al., 1991; Trull and Kurz, 1993; Shuster et al., 2004) retain neon, although we are not aware of quantitative measurements of diffusion kinetics in these minerals or in others that are potentially useful for exposure dating (e.g., feldspars).

Bruno et al. (1997) analyzed surface samples from the Antarctic Dry Valleys to study the consistency of exposure ages calculated from cosmogenic ^{21}Ne (^{21}Ne$_c$) in pyroxene and quartz, and in bulk dolerite (plagioclase and pyroxene). Whole-rock samples were deficient in ^{21}Ne$_c$ relative to pyroxene separates, suggesting that plagioclase feldspars incompletely retain Ne at Earth surface temperatures. Bruno et al. (1997), Schäfer et al. (1999), and Schäfer et al. (2000) measured ^{21}Ne$_c$ in pyroxenes at a variety of sites in the Antarctic Dry Valleys, and showed that (i) high temperatures are required (~1000 °C during 30 min to 1 h) to extract ^{21}Ne from pyroxene, and (ii) ^{21}Ne exposure ages from pyroxenes are more or less consistent with exposure ages determined otherwise. Thus, although these studies did not quantify neon diffusion kinetics, they show that (i) ^{21}Ne is retained at surface temperatures in pyroxene, and (ii) ^{21}Ne may not be retained at surface temperatures in plagioclase. On the other hand, Kober et al. (2005) showed that ^{21}Ne$_c$ concentrations in volcanic sanidine crystals were consistent with those in coexisting quartz, suggesting quantitative retention of Ne in sanidine. In addition, Poreda and Cerling (1992) found a constant ratio of ^{21}Ne concentration in volcanic plagioclase to that in coexisting olivine, suggesting quantitative retention in both minerals. To summarize, quantitative retention of cosmogenic Ne in olivine and pyroxene at Earth surface conditions seems nearly certain, but it is unclear if or when this is the case for feldspars.

Diffusive loss during natural reheating events to high temperature – such as forest fires (Reiners et al., 2007), proximal volcanic activity (Cooper et al., 2011), impact events at planetary surface (Shuster et al., 2010), and thermal conditions of meteorites (Min and Reiners, 2007) – have been shown to have perturbed the abundances of radiogenic noble gases in minerals. In principle, if the kinetics of ^{21}Ne diffusion in a particular mineral is known, the conditions of natural reheating events and their influence on cosmogenic ^{21}Ne abundances could also be quantitatively constrained. Neon can also be produced as a by-product of U and Th decay via secondary reactions with emitted α-particles, the primary production pathway being the ^{18}O(α, n)^{21}Ne reaction. Because the production of nucleogenic Ne is time-dependant, the (U–Th)/Ne system has been applied as a geochronometer (Basu et al., 2005, and Gautheron et al., 2006). Knowledge of Ne diffusion kinetics has implications for these applications and also for the behavior of noble gases in Earth's mantle (Albarède, 2008).

Few measurements of Ne diffusion kinetics in common minerals exist. In a recent review, Baxter (2010) summarizes the current literature that reports noble gas diffusion kinetics and highlights a near absence of published work on Ne. Shuster and Farley (2005) reported an activation energy (E_a) of 153 kJ/mol for ^{21}Ne diffusion in quartz, between 125 and 1400 °C; the estimated $\ln(D_o/a^2)$ is 15.9 $\ln(s^{-1})$. For comparison, the E_a for ^{3}He and ^{4}He is 84 kJ/mol and $\ln(D_o/a^2) \sim 11$ (Shuster and Farley, 2005); quartz more significantly retains neon than helium, by far more than expected from their difference in atomic mass (Shuster and Farley, 2005). Futagami et al. (1993) reported an E_a of 87.9 kJ/mol for ^{20}Ne diffusion in olivine, while reported values of E_a for He diffusion range broadly from 105 kJ/mol (^{3}He, Trull and Kurz, 1993) to 502 kJ/mol (^{4}He, Hart, 1984). According to these data and other studies of helium compiled by Baxter (2010), olivine appears – unexpectedly – to be more retentive to helium than to neon. We are not aware of published experimental data for neon diffusion in pyroxenes and feldspars. The objective of the present work is to study the diffusion kinetics of neon in three silicates: olivines, pyroxenes and feldspars.

2. METHODS AND SAMPLES

In most crystals, naturally occurring concentrations of cosmogenic or nucleogenic Ne are too low to permit detailed stepwise degassing experiments. To produce a measurable abundance of neon, which subject to various assumptions should produce a uniform spatial distribution of the diffusant, we irradiated olivine samples with 220 MeV protons at the Francis H. Burr Proton Therapy Center of the Massachusetts General Hospital (see Shuster and Farley, 2005) and irradiated pyroxene and feldspar samples with neutrons at the University of Oregon TRIGA reactor in the Cadmium-Lined In-Core Irradiation Tube (CLICIT). In olivine, the proton irradiation most likely produced ^{21}Ne and ^{22}Ne from various nuclear reactions on Si [i.e., Si(p,X)^{21}Ne, Si(p,X)^{22}Ne); Leya et al. (1998) and Shuster and Farley (2005)] and likewise Mg, where X

denotes the cumulative spallation production complementary to the Ne isotopes. Neutron irradiation produced ^{21}Ne and ^{21}Ne via nuclear reactions on Mg and Na, including the ^{24}Mg(n,α)^{21}Ne, ^{25}Mg(n,nα)^{21}Ne, ^{25}Mg(n,α)^{22}Ne, ^{26}Mg(n,nα)^{22}Ne and ^{23}Na(n,np)^{22}Ne reactions (e.g., see Cassata, 2011 for details regarding reaction cross sections). The abundance of neutron- or proton-induced neon depends on (i) the chemistry of the mineral (i.e., concentration and distribution of target elements), (ii) the flux and energy distribution of incident particles (i.e., n or p) and (iii) the total duration of irradiation.

Although samples are not significantly heated above room temperature during proton irradiation (Shuster et al., 2004), neutron irradiations in the CLICIT facility may heat samples to ~270 °C (Shuster and Farley, 2009). If neon diffusivity in a particular mineral is sufficiently high at ~270 °C, the spatial distribution of product ^{21}Ne or ^{21}Ne will not necessarily be uniform. The calculation of diffusion kinetics (below) assumes a spatially uniform distribution (Fechtig and Kalbitzer, 1966), however the potential effects of Ne diffusion during neutron irradiation can not be *a priori* established.

All samples used in diffusion experiments are compositionally homogeneous at the micron-scale, except sanidine crystals from the Fish Canyon Tuff (Fcs-A). SCOL is a gem-quality olivine (Fo_{90}) from San Carlos, Arizona, USA. PR-CPX ($En_{49.0}Fs_{1.6}Wo_{49.3}$) and PR-OPX ($En_{90.5}Fs_{9.3}Wo_{0.2}$) are gem-quality pyroxenes of unknown provenance (see Cassata et al. (2011) for additional details). ECCAb is Ca-rich anorthoclase ($An_{10.8}Ab_{71.8}Or_{17.4}$) megacryst from Easy Chair Crater, Lunar Craters Volcanic Field, Nevada, USA (Righter and Carmichael, 1993). MadOr is an orthoclase ($An_{0.2}Ab_{5.5}Or_{94.3}$) megacryst from a pegmatite from Itrongay, Madagascar. FCs-A is a high sanidine (zoned; core composition ~$An_1Ab_{27}Or_{72}$; Bachmann et al., 2002) from the Fish Canyon Tuff, Colorado, USA. The ECC and Mad samples both have minor mineral inclusions; the pyroxenes are inclusion-free.

2.1. Quantifying diffusion parameters

We used a method of stepwise degassing of single crystal fragments to quantify diffusion kinetics. By consecutively heating a sample to controlled temperatures, we allow a fraction of the total ^{21}Ne, ^{22}Ne and ^{20}Ne to diffuse from the sample in each heating step. We then calculated diffusion coefficients for each heating step from the proportion of total gas released and the duration of heating following Fechtig and Kalbitzer (1966), by assuming a Fickian diffusion mechanism and that diffusivity is isotropic. Isotropic diffusion of Ar in pyroxenes inferred by Cassata et al. (2011) may support this assumption. This method permits calculating the ratio D/a^2 without specifying the effective diffusion radius, a. By assuming that the physical grain size of an analyzed fragment defines a, the experimental results can be extrapolated to other dimensions.

Assuming that thermally-activated diffusion follows an Arrhenius law, E_a and D_o are related by the following equation:

$$\frac{D(T)}{a^2} = \frac{D_o}{a^2} \cdot e^{-E_a/RT} \quad (1)$$

In an Arrhenius plot [i.e., $\ln(D/a^2)$ versus T^{-1}] a linear relationship between calculated values for consecutive heating steps provides an estimation of $\ln(D_o/a^2)$ and E_a.

2.2. Experimental protocol

Stepwise heating experiments were performed under vacuum using either a 30 or 70 W diode laser ($\lambda = 810$ nm). Each crystal was placed in a Pt-Ir alloy tube (length ~1 mm, diameter ~0.7 mm) which was pinched closed at both ends to form an envelope. The envelope was placed in contact with a type-K thermocouple. The laser and thermocouple are then connected in a feedback loop with a PID temperature controller, which enables control and measurement of the sample temperature to within ±5 °C. To ensure spatial homogeneity in temperature, the laser beam was defocused so that it evenly covered the entire surface of the envelope. Photographs of the crystals were taken before and after the controlled heating steps, prior to final high-temperature fusion (see Supplementary file). The duration of each heating step varied between six minutes and two hours. Temperature intervals were designed in attempt to optimize quantification of E_a and D_o/a^2 as described above.

After heating, the extracted gas was expanded through an automated high-vacuum system and purified using a SAES getter. Neon was separated from other gases on a temperature-controlled cryogenic trap held at 70 K. The purified Ne was analyzed using the MAP-215 mass spectrometer in the BGC Noble Gas Thermochronometry Lab. Interferences on ^{22}Ne from CO_2^{++} and ^{20}Ne from Ar^{++} were corrected for by analyzing a spike of ^{39}Ar during the analysis of Ne (for full details see Balco and Shuster, 2009), although these corrections were negligible in the diffusion experiments. Total amounts of ^{21}Ne were quantified by peak height comparison to a manometrically-calibrated air standard; the air standard yielded Ne isotopic composition indistinguishable from atmospheric. The Ne sensitivity was linear within the measurement range of our analyses, established by varying the volume of the air standards.

Procedural blanks measured at room temperature were determined every 4–8 steps; all values report in Supplementary Table S1 are blank-corrected. The average magnitude of blank correction is ~10%, but typically is much higher for ^{21}Ne, and varies significantly depending on details of the heating schedule (i.e., controlling signal/blank). At the end of the experiments, samples were heated to between 1000 and 1400 °C for ~30 min (depending on the sample) to completely extract all gas and quantify the total amount of ^{20}Ne, ^{21}Ne and ^{22}Ne.

2.3. Cosmogenic ^{21}Ne measurements

In addition to the experiments with synthetically-produced Ne, we also investigated the retentivity of naturally occurring cosmogenic ^{21}Ne in feldspar by measuring cosmogenic ^{21}Ne in coexisting quartz and feldspar separates from a variety of rocks.

2.3.1. Samples for cosmogenic ^{21}Ne analyses

We analyzed quartz and sanidine phenocrysts in three samples from the Ammonia Tanks Tuff; rock was sampled from stable, slowly-eroding bedrock exposures on the crest of flat ridges and boulders on pediment surfaces south of Pahute Mesa and Yucca Mountain, Nevada, respectively. The Ammonia Tanks Tuff is a member of the Timber Mountain Group, which was erupted from the Timber Mountain caldera complex in the Southwestern Nevada Volcanic Field (Christiansen and Lipman, 1965; Christiansen et al., 1977). Its age is constrained by ^{40}Ar/^{39}Ar chronometry at 11.45 ± 0.03 Ma (Sawyer et al., 1994). The tuff is a metaluminous, compositionally zoned, welded ash-flow tuff (Broxton et al., 1989; Vogel and Aines, 1996; Mills et al., 1997). It grades from a rhyolite in its lower part to a crystal-rich (15–20% median modal total phenocryst content) trachyte with abundant sanidine (10–20%) and biotite (1–2%), common plagioclase and quartz (2–10%), and sparse clinopyroxene and sphene (<1%) in its upper part (Warren et al., 1989; Minor et al., 1993). Samples from this study were collected from this upper part. Large (up to 5 mm in diameter) sanidines and equant and euhedral quartz are characteristic of the unit. Broxton et al. (1989) presents whole rock geochemistry data for the Ammonia Tanks Tuff. Warren et al. (1989) document details of the mineralogy and petrology and Mills et al. (1997) summarize the major and trace element geochemistry of pumice fragments, mineral composition, and chemical zonation. Vogel and Aines (1996) report data on the geochemistry of its melt inclusions.

Second, we analyzed quartz and alkali feldspar in six samples from granitic boulders in the southern Transantarctic Mountains. These are glacially transported boulders deposited by an ice sheet advance of presumed Pliocene or older age (although apparent ^{21}Ne exposure ages reported here indicate a Miocene age), and the samples were collected by Bromley et al. (2010) for purposes of ^{10}Be exposure dating. We chose these samples because their long exposure duration ensured high concentrations of cosmogenic ^{21}Ne. The source area of these granites is unknown and presumably ice-covered; all are quartz-feldspar-biotite granites of similar mineralogy but varying texture and grain size. Alkali feldspar crystals in these samples are ~1 mm–1.5 cm in length and perthitic texture is visible in hand specimens.

2.3.2. Sample preparation for cosmogenic ^{21}Ne analyses

We separated quartz and feldspar fractions from both samples by crushing to a grain size (~0.5 mm) much smaller than the actual crystal size, and applying a variety of heavy liquid and magnetic separation methods. For the volcanic sanidine phenocrysts, we followed this with a brief etching in dilute HF to remove adhering groundmass. We visually inspected all feldspar separates and removed visible remaining contaminating grains. The quartz separates were further purified by repeated etching in dilute HF at 70 °C. In the Supplementary File, Table S3 shows the major element chemistry of the feldspar separates. We then extracted ^{21}Ne in several heating steps as described in Balco and Shuster (2009); Tables S2 and S4 show results.

3. RESULTS

3.1. Diffusion experiment results

Three representative Arrhenius plots (an olivine, a pyroxene and a feldspar sample), are shown in Fig. 1. Complete datasets and Arrhenius plots for all samples are shown in the supplement (Table S1). For each data point (i.e., for each heating step), the analytical uncertainty in the abundance of blank-corrected ^{21}Ne or ^{22}Ne was propagated into the calculated values of $\ln(D/a^2)$. For each sample, values of E_a and $\ln(D_o/a^2)$ were determined by calculating an error-weighted linear regression (Eq. (1)) and a reduced chi-squared χ_v^2 mistfit statistic. The apparent diffusion parameters and sample dimensions are summarized in Table 1. Two regressions were calculated: one including all of the data and one to a best-fit subset of the data, which were chosen on the basis of several criteria. If an entire dataset did not present a simple Arrhenius relationship, our objective was to minimize the misfit between the data and the regression, while including as many consecutive steps as possible in attempt to isolate the portion of the experiment that exhibits a linear Arrhenius relationship. The selected data were required to include one or two sets of sequential heating steps, including increasing and decreasing temperatures. Another criterion was the reproducibility of the heating steps. For sequential isothermal steps, data were included when the difference between the two values of calculated $\ln(D/a^2)$ is within 1 natural log unit.

In most instances, the Arrhenius arrays were not perfectly linear (discussed below), although unambiguous differences are evident between mineral groups. Using the selection criteria described above, we find that olivine E_a ranges from 360 ± 30 to 367 ± 8 kJ/mol [$\ln(D_o/a^2)$ ranges from 20 ± 1 to 21 ± 3 ($\ln(s^{-1})$), respectively]. According to the regressions of entire ^{21}Ne datasets (^{22}Ne datasets, respectively), olivine E_a ranges from 181 ± 3 to 215 ± 2 kJ/mol (260 kJ/mol) and $\ln(D_o/a^2)$ ranges from 4 ± 0.3 to 7 ± 0.1 (11 ± 1) ($\ln(s^{-1})$). Best-estimates for ^{21}Ne diffusion kinetics in pyroxenes are as follows: E_a ranges from 292 ± 1 to 480 ± 1 kJ/mol and $\ln(D_o/a^2)$ ranges from 14 ± 0.1 to 33 ± 0.1 ($\ln(s^{-1})$), with the higher activation energies and frequency factors corresponding to orthopyroxene. Best-estimates for ^{22}Ne diffusion kinetics (^{21}Ne, ECCAb sample) in feldspar are as follows: E_a ranges from 83 ± 1 to 115 ± 14 kJ/mol (65 ± 5) and $\ln(D_o/a^2)$ ranges from 3 ± 0.2 to 13 ± 4 (-0.4 ± 1) ($\ln(s^{-1})$).

In many extractions, the ^{22}Ne signal in the olivine and orthopyroxene experiments approached the analytical detection limit (Table S1), and is therefore sensitive to blank corrections. Although in some cases we calculate different Arrhenius parameters for ^{21}Ne and ^{22}Ne by linear regression, we do not consistently find differences between the calculated values of D/a^2 for each isotope. We believe the isotopic differences shown in Table 1 are primarily due to differences in data quality and the influence of our regression criteria, rather than true differences in the diffusion kinetics of each isotope. For these reasons, in the cases of olivine and orthopyroxene, we only consider subset regressions to ^{21}Ne data.

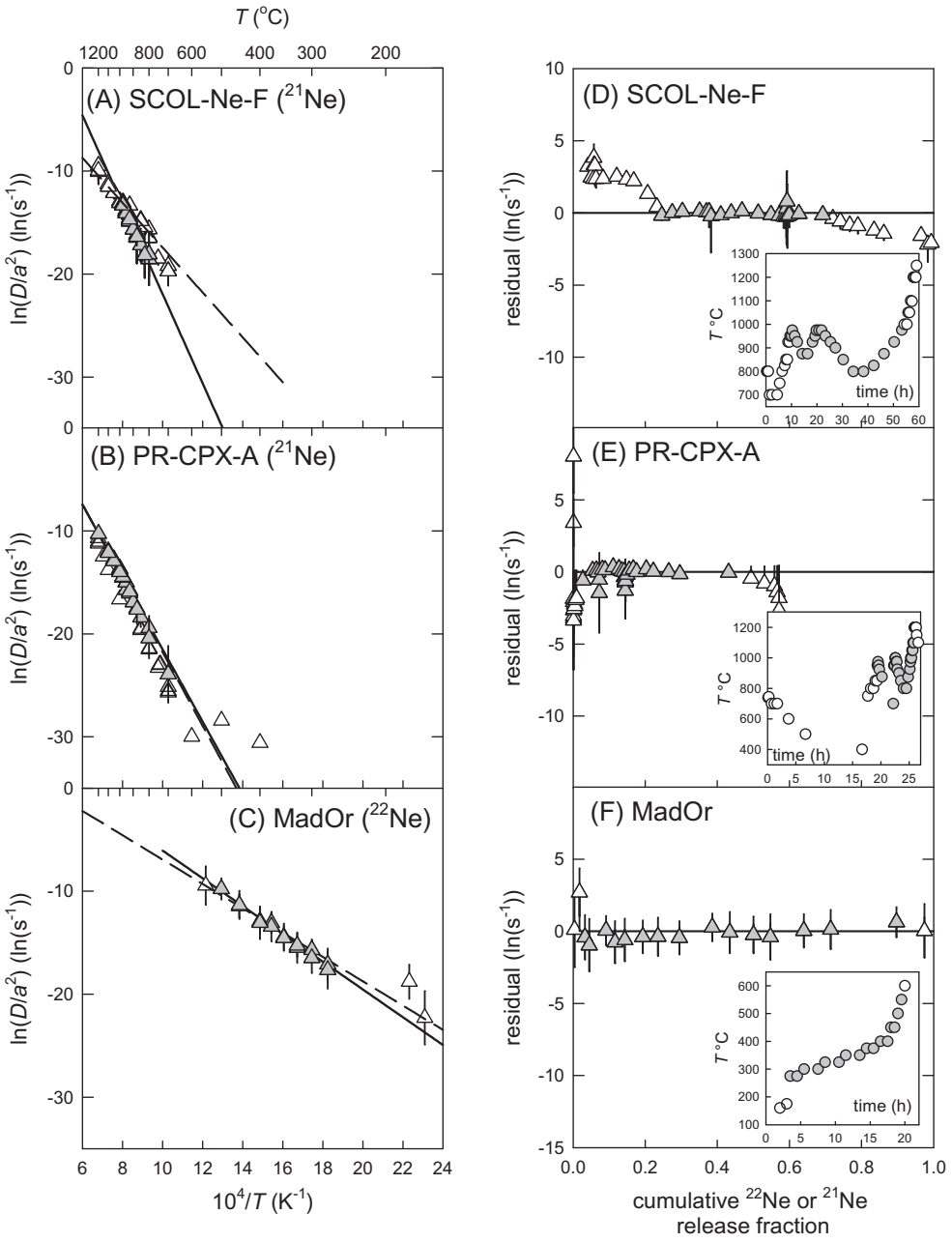

Fig. 1. Three example Arrhenius plots; sample (A) San Carlos olivine, (B) clinopyroxene and (C) orthoclase. (A–C) Shown as open symbols are the calculated values of $D/a^2 \pm 1$ s.d. following equations by Fechtig and Kalbitzer (D is diffusivity, a is the characteristic diffusive lengthscale, radius, of a spherical geometry), plotted against reciprocal of absolute temperature T. Dashed lines are error-weighted linear regressions to each complete dataset. Filled points in gray indicate those selected for regression based on criteria discussed in the text; solid black line indicates corresponding regression. (D–F) Symbols are deviation from the subset regressions shown in left hand panels plotted against the cumulative fraction of released Ne. Filled points in gray indicate the selected data. Inset panels illustrate the heating schedule. Corresponding figures for all experiments are shown in the Supplement file (Fig. S1).

Due to the complexity observed in Arrhenius plots, it is important to note that the regression statistics reported in Table 1 most likely underestimate the true uncertainty in kinetic parameters. Nevertheless, we found that the activation energies for neon diffusion in olivines and pyroxenes are clearly higher than that for feldspars, by at least a factor of 2. The activation energies for neon diffusion in orthopyroxenes are higher than for clinopyroxene, by a factor of ~1.5, in these experiments.

During these experiments, it is important that the samples remain chemically stable and physically intact. Following the controlled-heating extractions we visually inspected each sample with an optical microscope. In some cases we observed subtle changes in the luster of the crystals, and

Table 1
Summary of Ne diffusion parameters.

	Sample	SR[a] (μm)	Isotope	T range[b] (°C)	E_a [c] (kJ/mol)	(±)	$\ln(D_o/a^2)$ [c] ($\ln(s^{-1})$)	(±)	Subset E_a [d] (kJ/mol)	(±)	Subset $\ln(D_o/a^2)$ [d] ($\ln(s^{-1})$)	(±)	Apparent D_o [e] (cm^2/s)
Olivine													
	SCOL-Ne-E	498	^{21}Ne	700–1250	215.0	1.5	6.7	0.1	369.9	7.7	20.2	0.7	1.5×10^{6}
			^{21}Ne		260.0	20.4	10.7	1.3					
	SCOL-Ne-F	503	^{21}Ne	700–1200	181.1	3.1	4.4	0.3	360.4	30.1	21.4	2.9	5.0×10^{6}
Pyroxene													
Orthopyroxene	PR-OPX-D	376	^{21}Ne	400–1200	384.6	0.2	23.7	0.0	469.2	0.6	33.0	0.1	2.9×10^{11}
			^{21}Ne		326.4	1.0	18.4	0.1					
	PR-OPX-E	202	^{21}Ne	500–1200	462.1	0.4	30.3	0.0	479.6	0.5	32.0	0.1	3.1×10^{10}
Clinopyroxene	PR-CPX-A	140	^{21}Ne	600–1200	298.1	0.7	14.1	0.1	292.2	0.8	13.6	0.1	1.6×10^{2}
Feldpsar													
Anorthoclase	ECCAb	775	^{21}Ne	175–700	64.6	5.1	−0.5	1.0	64.5	5.1	−0.4	1.0	3.9×10^{-3}
			^{21}Ne		83.4	0.6	2.8	0.1	83.2	0.8	2.8	0.2	1.0×10^{-1}
Sanidine	FCs-A	452	^{21}Ne	125–600	62.6	3.7	0.0	0.8	114.8	14.3	12.8	3.5	7.1×10^{2}
Orthoclase	MadOr	531	^{21}Ne	125–700	98.2	27.7	4.9	5.3	112.1	34.4	7.4	6.5	4.7×10^{0}

Note: all reported uncertainties are solely from error-weighted linear regressions likely underestimate the true uncertainty in these parameters.

[a] Radius of a sphere with approximately equivalent surface area to volume ratio, estimated from measured cross-dimensions of the analyzed fragments. Images of analyzed fragments appear in the Online Supplement.

[b] T corresponds to range in heating steps (lowest and highest temperatures), excluding the final high-temperature extraction.

[c] These values were calculated from each entire dataset without consideration of reproducibility at a given temperature.

[d] The subset values are those calculated from a subset of data, selected according to criteria discussed in the text, which we consider to be best-estimates. Due to relatively low signal/noise, we do not consider the ^{21}Ne results for olivine and pyroxene in these subset estimates.

[e] By assuming the effective radius of analyzed fragments (SR) defines "a", we calculate the apparent values of D_o.

in two cases a change in the geometry (Supplementary Fig. S2).

3.2. Cosmogenic ^{21}Ne results

Results of step-degassing analysis of naturally occurring feldspar and quartz samples are given in Table 2 and Tables S2–S4 and shown as three-isotope diagrams in Fig. 2 and Fig. S3. Isotope ratios of all heating steps for all samples of both minerals were consistent with two-component mixing between atmospheric and cosmogenic Ne. Our results for quartz fall on the well-established mixing line for quartz of Niedermann et al. (1993) (Fig. S3). Kober et al. (2005) derived an air-cosmogenic mixing line for sanidine, and our results from sanidine are consistent with this mixing line (Fig. 2). Because sanidine and quartz are expected to contain small amounts of U and Th, a small inventory of nucleogenic Ne must be present in both minerals. However, Ne isotope ratios provide no evidence for significant nucleogenic Ne in either mineral, so we assume that nucleogenic Ne is insignificant, and calculate cosmogenic ^{21}Ne concentrations according to a two-component deconvolution (Niedermann, 2002). Also in agreement with the results of Kober et al. (2005), all cosmogenic ^{21}Ne in our sanidine samples was extracted in 370 and 740 °C heating steps, and Ne extracted in a high-temperature step was indistinguishable from atmospheric composition. For our alkali feldspar samples, on the other hand, 3–15% of total cosmogenic ^{21}Ne was extracted in high-temperature steps. We see no obvious explanation for this discrepancy, although one possible explanation would be the presence of trace amounts of a more retentive mineral in the alkali feldspar separates.

4. DISCUSSION

As noted above, most Arrhenius arrays are not linear which suggests either (1) crystal fragments comprise multiple diffusion domains, (2) structural changes occurred during the course of step-heating experiments, (3) multiple diffusion mechanisms exist (e.g., diffusion paths related to dislocations or other crystallographic defects), and/or (4) initial concentration distributions were heterogeneous (presumably due to diffusive loss during irradiation). However, although the regressions are relatively imprecise, they reveal unambiguous, order-of-magnitude differences in diffusion kinetics between the samples.

4.1. Neon diffusion in olivine

Each olivine experiment produced a complex Arrhenius plot. Although our best-fit estimates of E_a from the two experiments are in good agreement with one another (Table 1), the estimates from subset ^{21}Ne data result in significantly higher activation energies than those calculated from the entire datasets: 215 ± 2 versus 370 ± 8 kJ/mol (sample SCOL-Ne-E, Fig. 3); 181 ± 3 versus 360 ± 30 kJ/mol (sample SCOL-Ne-F, Fig. 1). Furthermore, the subset regressions correspond to only ~40% of the total ^{21}Ne contained in each crystal. Although our regressions assume that a single Arrhenius relationship has been isolated, the complex patterns may reflect the occurrence of several diffusion pathways or sub-grain domains. For example, if more than one diffusion domain size exists within these samples, the apparent E_a determined from a mixture of diffusion domain may underestimate the actual value for any one domain (Lovera et al., 1991). Additional experiments

Table 2
Cosmogenic ^{21}Ne concentrations in coexisting quartz and feldspar separates.

Sample	[^{21}Ne] in quartz (10^6 atoms g^{-1}) [a]	[^{21}Ne] in feldspar (10^6 atoms g^{-1})[a]	Ratio Fsp/Qtz (measured)	Model P (sample)/P (anorthite)[b]	Ratio Fsp/Qtz (normalized to anorthite)[b]	Apparent ^{21}Ne exposure age (Ma)[c]
Ammonia Tanks Tuff						
QA774	9.16 ± 0.60	12.81 ± 0.76	1.40 ± 0.12	1.18	1.19 ± 0.11	0.148 ± 0.0097
QA767	39.9 ± 1.2	48.37 ± 1.2	1.212 ± 0.047	1.12	1.078 ± 0.042	0.60 ± 0.018
061808A	8.90 ± 0.44	11.44 ± 0.84	1.29 ± 0.11	1.08	1.19 ± 0.11	0.25 ± 0.012
Transantarctic Mountains granites						
011-QZH	1134 ± 19	746 ± 20	0.658 ± 0.021	1.18	0.559 ± 0.018	10.57 ± 0.18
063-QZH	266.2 ± 7.9	169 ± 17	0.635 ± 0.067	1.13	0.564 ± 0.059	3.079 ± 0.091
074-QZH	473 ± 14	428 ± 17	0.905 ± 0.045	1.09	0.826 ± 0.041	4.45 ± 0.13
114-PGN	226.2 ± 5.7	182 ± 13	0.805 ± 0.061	1.11	0.722 ± 0.055	1.59 ± 0.04
164-TLL	866 ± 17	550 ± 23	0.635 ± 0.029	1.20	0.530 ± 0.024	6.00 ± 0.12
167-TLL	1037 ± 27	952 ± 21	0.918 ± 0.031	1.20	0.766 ± 0.026	6.95 ± 0.18
Chilean ignimbrites from Kober et al. (2005, 2007) and Ivy-Ochs et al. (2007)						
CN-5S	200.1 ± 6.2	327.4 ± 6.3	1.636 ± 0.060	1.36	1.207 ± 0.044	1.900 ± 0.059
CN19S	320.3 ± 4.8	399.7 ± 6.7	1.248 ± 0.028	1.28	0.974 ± 0.022	4.070 ± 0.061
CN23S	226.4 ± 4.2	378 ± 7.7	1.670 ± 0.046	1.34	1.242 ± 0.034	2.135 ± 0.040
CN113S	4.80 ± 0.60	6.60 ± 0.60	1.39 ± 0.23	1.23	1.13 ± 0.19	0.0245 ± 0.0031
CN201S	283.6 ± 8.1	435.8 ± 7.4	1.537 ± 0.051	1.22	1.259 ± 0.042	2.459 ± 0.070

[a] Complete step-degassing data appear in the Supplementary material.
[b] Calculated from model elemental production rates of Kober et al. (2005). See Supplementary material.
[c] Calculated from ^{21}Ne concentration in quartz separate. See Supplementary material.

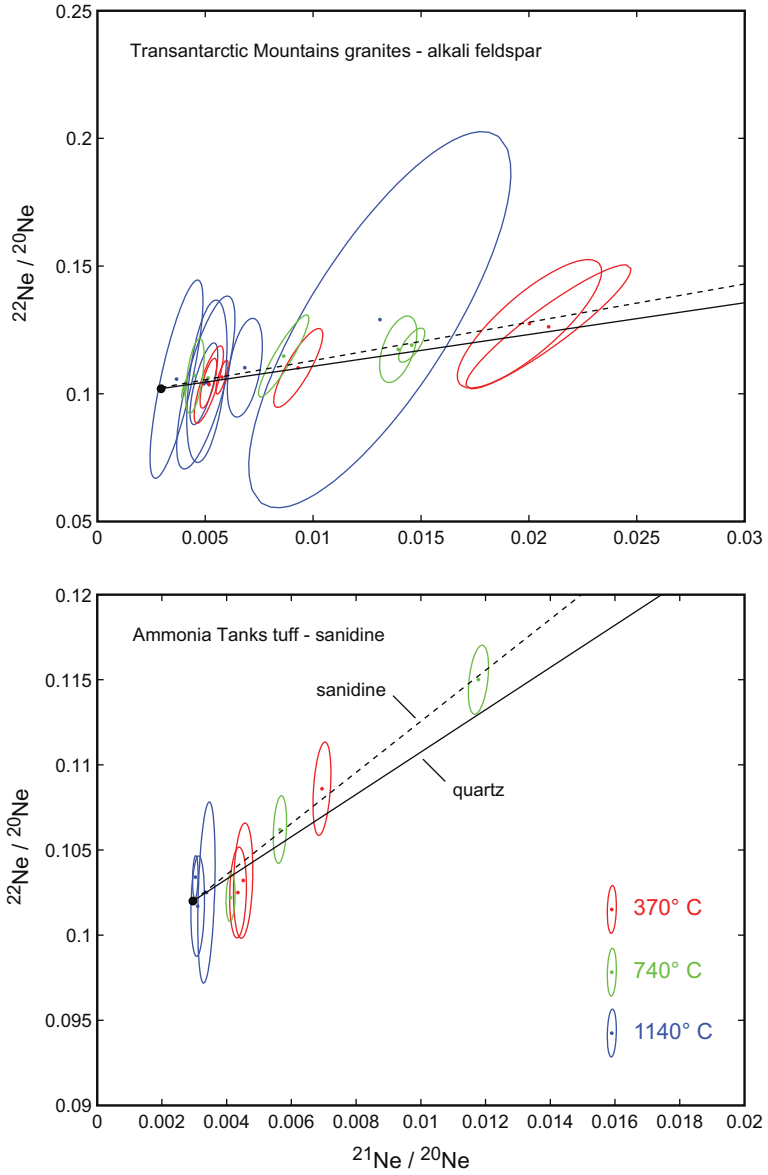

Fig. 2. Isotopic composition of naturally-occurring Ne extracted in step-degassing analysis of feldspar samples (see Table S2). Ellipses are 68% confidence regions. The black circle shows the composition of atmospheric Ne, the solid line is the air-cosmogenic mixing line for quartz (Niedermann et al., 1993), and the dashed line is the air-cosmogenic mixing line for sanidine proposed by Kober et al. (2005). Comparable figures for the quartz samples are shown in Fig. S3.

would be required to rule out the possibility of sub-domain diffusion.

The surface texture of sample SCOL-Ne-E was modified at some point during the experiment (see Fig. S2A). A modification to the crystal during the experiment is plausible and may potentially introduce bias in an Arrhenius plot. Our experiments were performed under vacuum between 700 and 1250 °C; with the highest temperature below the melting point. Is it possible that only the surface was altered [e.g., possibly due to a reaction at high temperature Lemelle et al. (2001)]. However, the surface of SCOL-Ne-F shows no sign of modification visible with optical microscopy. Although we can not completely exclude the possibility of surface reactions, agreement between the two experiments suggests that the phenomenon associated with observed changes at the surface of SCOL-Ne-E are unlikely to have strongly influenced both sets of results. Barring the aforementioned complexities, the apparent kinetics of Ne diffusion from our experiments is reproduced in different aliquots, and is significantly different from previous results in olivine reported by Futagami et al., 1993.

4.2. Neon diffusion in pyroxene

The estimated activation energy (from subset arrays; Table 1) for Ne diffusion in pyroxene is high (from ~292 to 480 kJ/mol), causing Ne to be strongly retained within pyroxene at and near Earth-surface temperatures and

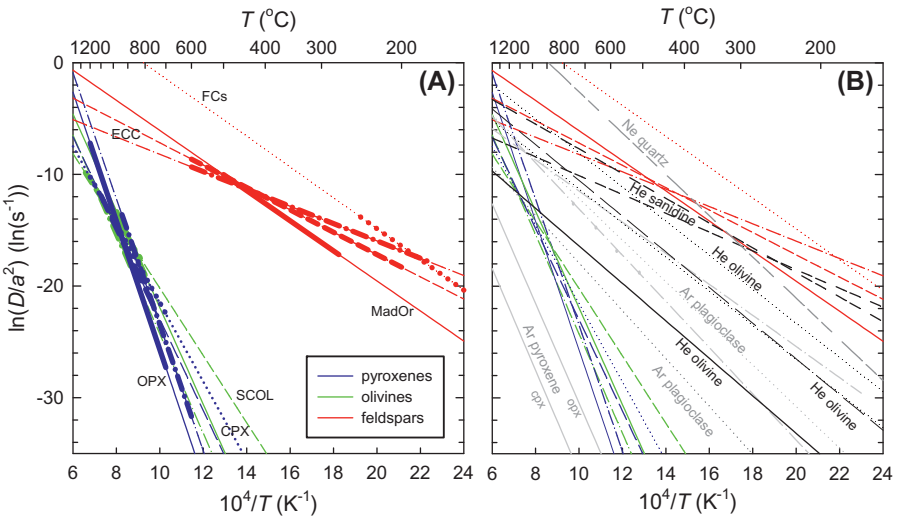

Fig. 3. Summary of Arrhenius relationships for neon diffusion in olivine, pyroxenes and feldspars. (A) Colored lines are results for San Carlos olivine (green), pyroxenes (blue), and feldspar (red). The apparent kinetics of Ne diffusion in feldspars are shown as follows: Madagascar low-sanidine (MadOr, ^{21}Ne, solid), Fish Canyon sanidine (FCs, ^{21}Ne, dotted), Easy Chair Crater anorthoclase (ECCAb, ^{21}Ne, dash-dot; ^{21}Ne, dash). San Carlos olivine sample SCOL-Ne-F is shown as solid line (^{21}Ne); SCOL-Ne-E is shown as dash-dot line (^{21}Ne) and dashed line (^{21}Ne). The results for pyroxene are shown as follows: Orthopyroxene PR-OPX-D (^{21}Ne dash-dot, ^{21}Ne dash), PR-OPX-E (^{21}Ne solid); clinopyroxene PR-CPX-A (dotted). Thick line segments correspond to the experimental temperature ranges of regressed datasets. (B) Shown for reference in black (He) and gray (Ne, Ar) are published results for ^{21}Ne diffusion in quartz (from Shuster and Farley, 2004), Ar diffusion in pyroxenes (Cassata et al., 2011), Ar diffusion in plagioclase (regolith, Shuster et al., 2010, shown by the dashed-dotted line; Cassata et al., 2009, shown by the dotted line), He diffusion in sanidine (Lippolt and Weigel, 1988) and He diffusion in olivine (Shuster et al., 2004, shown by the solid line; Blard et al., 2008, shown by the dotted lines; Tolstikhin et al., 2010, shown by the long-dashed line). Note that data for Ar diffusion in plagioclase are not representative of all plagioclase compositions. D is diffusivity, a is the characteristic diffusive lengthscale, radius, of a spherical geometry, plotted against reciprocal of absolute temperature T. (For interpretation of the references to color in this figure legend, the reader is referred to the web version of this article.)

during brief reheating events to hundreds of degrees. Furthermore, the activation energy for neon diffusion in the orthopyroxenes appears to be higher than that of clinopyroxenes PR-CPX-A. The cumulative heating duration of each experimental was similar: 27 h (PR-CPX-A), 30 h (PR-OPX-D) and 21 h (PR-OPX-E); prior to final fusion, the penultimate temperature was 1200 °C for each. Although the heating schedules were somewhat different (Supplementary Table S1D and S1E), by the 1200 °C step, the orthopyroxenes had released 90% of their neon, while sample PR-CPX-A had released only 60%.

We observed that two orthopyroxene samples (PR-OPX-D and PR-OPX-E) were broken after the analysis. We believe that the breaking most likely occurred sometime during heating, as possibly indicated by the upward kink in the Arrhenius plot for PR-OPX-E (Fig. S1D) at ~900 °C. The sample was introduced very carefully in the Pt-Ir envelope so the likelihood of breaking before the experiment is very low, but cannot be totally excluded. However, clinopyroxene sample PR-CPX-A was clearly intact with a common geometry both before and after analysis. The higher diffusivity in the orthopyroxenes and the fact that both released a larger fraction of Ne by 1200 °C may be related to the crystals having broken early during the analysis, resulting in fragments smaller than the analyzed clinopyroxene (i.e., resulting in a higher apparent value of D_o/a^2). Sample PR-OPX-D was broken in two fragments with an approximate size half that of the whole sample. Sample PR-OPX-E was broken in several fragments; the largest was ~1/3 of the whole sample. Alternatively, the crystals may have broken late in the experiment (e.g., during the highest-temperature steps) in which case the apparent values of D_o/a^2 reflect differences in the material properties. Provided that the orthopyroxenes did not fracture gradually –which seems unlikely – the difference in the activation energy of neon diffusion in clinopyroxene and orthopyroxene may reflect either small differences in physical properties (clinopyroxenes have a slightly higher density than orthopyroxenes) or lattice geometry.

Our observed range in apparent activation energy spans values reported by Cassata et al. (2011) for Ar diffusion in the same pyroxenes: ~371–379 kJ/mol. However, the maximum values ~480 kJ/mol are higher than most previous values reported for noble gas diffusion (Baxter, 2010). Based on their differences in size and mass, we might expect that Ne diffusion should have a lower activation energy than Ar diffusion in a particular mineral, although these relationships are not well understood. Since we can not rule out the possibility that our subset data selection has somewhat overestimated E_a for Ne, further experimentation involving simultaneous degassing of both Ne and Ar are required to more fully evaluate the relative activation energies of the gases.

4.3. Neon diffusion in feldspar

The neon diffusivities observed below ~800 °C in different feldspar samples are consistently higher than in olivine and pyroxene, and are generally consistent with one another. The apparent activation energies of ^{22}Ne diffusion in feldspar (~63–98 kJ/mol; regressions to entire datasets) are systematically and significantly lower than those observed for olivine and pyroxene.

Sample FCs-A (sanidine) presents a particularly complex Arrhenius plot (Supplementary Fig. S1G): the activation energy calculated for the first heating steps (from 125 to 250 °C) is 114.8 ± 14.3 is significantly higher than that calculated from the entire dataset: 62.6 ± 3.6 kJ/mol. Core to rim electron microprobe traverses reveal Na depletion toward grain margins (Bachmann et al., 2002), which in turn is expected to yield low ^{22}Ne concentrations at grain margins, since the production of ^{22}Ne during irradiation depends on the distribution of the target nuclide (^{23}Na). Moreover, FCs was the least retentive sample analyzed; 50 h of heating in a reactor at 270 °C could have caused 28.8% loss of ^{22}Ne. Samples with initially diffusive concentration distributions would yield lower than expected D/a^2 values at low T, which may partially explain the observed Arrhenius plot. The non-zoned samples (anorthoclase = ECCAb and K-feldpsar = MadOr) present more linear arrays (Fig. SF1H and SF1F). The E_a value of ECCAb is slightly lower than that of MadOr (from ^{22}Ne).

The texture of sample FCs-A does appear to have been modified during heating (*cf* Supplementary Fig. S2). Sample MadOr was broken in two parts, but mostly likely happened after the experiment, as the metallic envelope containing the crystal was opened. The Arrhenius plot suggests one simple apparent diffusion pathway (Fig. 1C). If the crystal had been broken during the heating, we would expect a more complex Arrhenius array.

4.4. Comparing the kinetics of Ne diffusion between minerals and other noble gases

Variations in E_a attest to large differences in the temperature dependence of diffusivity in the three studied mineral groups. Fig. 3 summarizes our best estimates from the present work, with published relationships for Ne (Shuster and Farley, 2004), He (Lippolt and Weigel, 1988; Shuster et al., 2004; Blard et al., 2008; Tolstikhin et al., 2010) and Ar (Cassata et al., 2009, 2011; Shuster et al., 2010) for comparison. Ne diffusivity at Earth surface temperature in feldspars is clearly higher than in olivine and the pyroxenes when extrapolated from the experimental conditions. Neon diffusion in feldspar has apparent activation energy between ~63 and 98 kJ/mol (regression to all data) whereas the range in E_a for olivine and pyroxenes ranges from ~180 to values above 400 kJ/mol. We also find this difference magnitude in the sub-selected data (Table 1). In Fig. 3B we compare Ne diffusion parameters to previously published results for He and Ar diffusion in pyroxenes, olivines, and feldspars. As with our Ne results, it is interesting to note that Ar diffusion in pyroxene also has higher activation energy than in feldspars. However, the difference in E_a between these minerals for Ar diffusion [ΔE_a ~100–220 kJ/mol, with exception of Thomas et al. (2008) who reported a low E_a for argon diffusion in enstatite (32 kJ/mol)] appears to be much smaller than what we observe for Ne (ΔE_a ~180–415 kJ/mol). This comparison suggests the influence of physical differences between Ar and Ne (e.g., the van der Waals radius). We also find that the E_a for Ne diffusion in the feldspars is significantly lower than the E_a for He diffusion in olivine (ΔE_a ~360), suggesting the importance of mineralogical control on noble gas diffusion kinetics.

The relatively high activation energy for Ne diffusion in pyroxene is consistent with previous studies of both Ar and He diffusion in pyroxene. Interestingly, the apparent activation energy for Ne diffusion is quite similar to those reported for Ar diffusion by Cassata et al. (2011): 379.2 ± 4.2 kJ/mol in clinopyroxenes and 371.0 ± 6.0 kJ/mol in orthopyroxenes (measured between 850 and 1350 °C), although the diffusivities (D) are about an order of magnitude faster at a given temperature for Ne than for Ar (Fig. 3B). The activation energy for He diffusion in augites was estimated to be ~116 and 124 kJ/mol by Lippolt and Weigel (1988) between 730 and 1400 °C.

Differences in neon diffusivity between and within mineral groups are likely related to effective diffusion radius, crystal structure, crystal chemistry, defect density, state of order, water content, and other factors. One of the primary controls on atomic diffusion of noble gases within solids may simply be the available free space, *a fortiori* for gases: as they have a fast null reactivity, i.e., the probability that neon becomes bounded to (or reacts with) atoms constituting the crystal lattice is negligible, and neon diffuses without being affected by the chemical nature of the crystal; consequently, neon diffusion should be mainly controlled by geometry and lattice node density of crystals, i.e., ionic porosity of Fortier and Giletti (1989). Ionic porosity is the volumic fraction not occupied by ions in a mineral unit-cell (Dowty 1980); a crystal with a low ionic porosity has less available space for diffusion. After Fortier and Giletti (1989), the approximate ionic porosities at surface temperature of olivine (forsterite), clinopyroxene (diopside) and K-feldspar (orthoclase) are 34.9%, 34.3% and 44.7%; ionic porosity of plagioclase feldspar varies between 44.1% (albite) and 44.5% (anorthite). Our results show a negative apparent correlation between ionic porosity and E_a for the ferromagnesian minerals (pyroxene and olivine) and feldspars. It seems plausible that diffusivity at a certain temperature may be correlated with ionic porosity, at least for an inert gas; Zhao and Zheng (2007) compiled argon diffusion kinetics in various minerals and reported a linear correlation between E_a and ionic porosity. However, the physical mechanism that would produce correlation with E_a is not obvious. Also, the apparent E_a for olivine is consistently lower than that of pyroxene, which suggests that ionic porosity is not the sole controlling factor. Furthermore, differences in ionic porosity (and E_a) alone do not obviously predict convergence of diffusivity at high temperature.

Although some evidence for anisotropy in the diffusion of noble gases in these silicates and other minerals has been

documented (Cherniak and Watson, 2011; Baxter, 2010), the design of our experiments and relative imprecision of the results do not permit us to draw quantitative conclusions about whether Ne diffusion in these phases is purely isotropic. However, significant anisotropy through a bulk crystal would *a priori* lead to several diffusion velocities and the dominant results visible in an Arrhenius plot would be due to the fastest diffusion; we can not exclude the possibility that our results are somehow influenced by anisotropy. Although Cassata et al. (2011) also found no significant evidence of anisotropic diffusion of argon in oriented fragments of the same pyroxenes as in this study, anisotropy in the ionic porosity, as introduced by Cherniak and Watson (2011), could potentially cause anisotropy in Ne diffusion in pyroxene; further experimentation is required to interrogate these potential effects.

A physical interpretation of the parameter D_o/a^2 may reflect differences in a fundamental material property (i.e., D_o), or the effective diffusion radius. While our experiments were not designed to establish whether the domain is defined by the physical crystal dimensions for Ne diffusion, Cassata et al. (2011) showed the physical grain dimensions defines the limiting diffusive length-scale for Ar diffusion in PR-OPX and PR-CPX. Likewise, using detailed UV-laserprobe traverses, Wartho et al. (1999) showed the Ar diffusion in MadOr occurs at the grain scale. Although the role of crystal or grain size has been demonstrated for Ar diffusion in these phases, further experiments are required to fully assess this for Ne. However, in our calculations below, we assume that the macroscopic dimensions of analyzed crystals ultimately limit the effective diffusion domain for neon, and that the apparent values of D_o/a^2 scale with crystal size.

In Fig. 4 we show Arrhenius relationships by assuming that "a" is equal to the effective spherical radii given in Table 1 [i.e., $\ln(D)$ versus $1/T$]. Under this assumption, we should minimize the influence of grain size on the results; this plot more directly compares the kinetics of each experiment and the values reported in the literature. After correcting for grain size, it is apparent that at low temperatures Ne diffusivities in feldspars are orders of magnitude higher than in pyroxene and olivine, and also higher than in quartz. Olivine is the only mineral that we can compare with published results. Futagami et al. (1993) reports an activation energy that is a factor of ~2–4 lower than our results and an Arrhenius relationship that clearly differs even at similar experimental temperatures. Although the large apparent differences may be related to differences in the analyzed olivine, since Futagami et al. (1993) employed a very different technique involving energetic implantation of Ne ions, it is also possible that differences may reflect unidentified analytical artifacts related to radiation damage or aggregation of Ne into bubbles, particularly at higher Ne doses. Additional work involving Ne ion implantation on the same samples used for bulk degassing may be required to fully assess the apparent discrepancies.

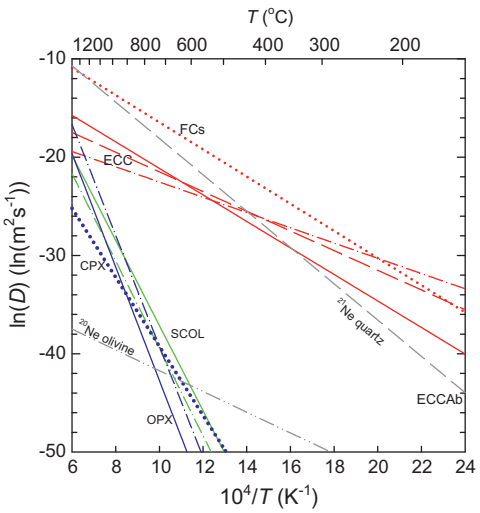

Fig. 4. Summary of Arrhenius relationships assuming the effective radii (SR) of the samples in our study approximate the diffusion domain radii a (Table 1). The line styles corresponding to samples are the same as in Fig. 3. Also shown for reference are the relationships for ^{21}Ne diffusion in quartz (Shuster and Farley, 2005) and ^{20}Ne diffusion in olivine (Futagami et al., 1993, as estimated by Baxter, 2010).

4.5. Retentivity of Ne at low temperatures

In order to establish whether a mineral can be used for cosmogenic ^{21}Ne observations, it is necessary to assess whether cosmogenic ^{21}Ne is quantitatively retained. Fig. 5 shows calculations of Ne retention over a period of 10 ka (a time period of interest for cosmogenic-nuclide exposure dating), for a range of grain sizes and temperatures,

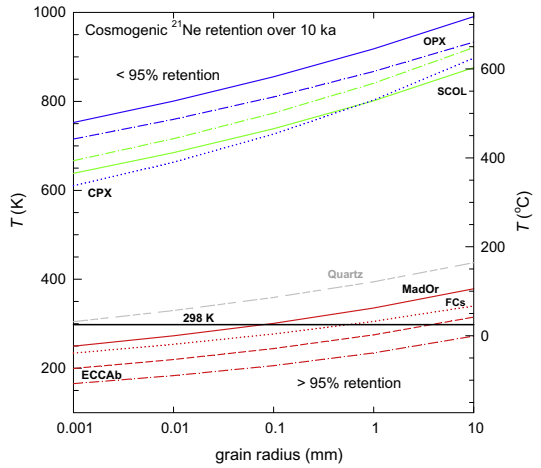

Fig. 5. Apparent Ne retentivity in olivine, pyroxenes and feldspars. The curves show the threshold temperatures at which 5% diffusive loss would occur in olivine (green curves), pyroxenes (blue curves), and feldspars (red curves) as a function of grain radius for isothermal accumulation duration of 10,000 years. The line style (solid, dashed, dotted) corresponding to the samples is the same as in Fig. 3. The calculation is based on the accumulation-diffusion equation as described in Wolf et al. (1998), modified for cosmogenic production of ^{21}Ne and uses the experimental results summarized in Table 1. The calculation assumes spherical diffusion geometry and a zero concentration boundary condition. Shown for reference as a solid horizontal line is 25 °C. (For interpretation of the references to color in this figure legend, the reader is referred to the web version of this article.)

according to the method used by Shuster and Farley (2005) after Wolf et al. (1998). These calculations include a constant production rate and temperature-dependent diffusion of Ne in a mineral grain over a specified time period. They relate temperature and mineral grain size to the amount of Ne produced during that time period which is lost by diffusion. Thus, one can compute the temperature for which a crystal of a particular size retains 95% of its ^{21}Ne (or ^{22}Ne) content for a given duration at a constant temperature, or assume the temperature and degree of retention to calculate the theoretical corresponding grain size. The calculation uses the E_a and $\ln(D_o/a^2)$ determined from our experiments, which implies an assumption that the diffusion parameters we estimated at laboratory temperatures (>100 °C) can be extrapolated to lower temperatures. As in Fig. 4, the diffusion radius in the experiment (a) was assumed equal to the radius of a sphere with equivalent surface area to volume ratio, as estimated from measured cross-dimensions of the analyzed samples (SR in Table 1); a is assumed to be unique (i.e., a single domain diffusion), allowing us to scale D/a^2 to different grain radii (1 μm–10 mm).

These calculations reveal that olivine and the pyroxenes will quantitatively retain ^{21}Ne when the temperature is less than ~600 K, for the grain size range considered. Orthopyroxene (sample PR-OPX-E) is the most Ne-retentive. The high activation energy that we observe for olivine and pyroxene implies that retention is primarily sensitive to temperature and less sensitive to grain size. In contrast, the calculations predict that feldspars will quantitatively retain neon at Earth surface temperatures, on timescales relevant for exposure dating, only for large grain sizes (radius >0.1–1 mm). Smaller grains will lose significant amounts of Ne by diffusion.

These results indicate that diffusion kinetics of olivine and pyroxenes are clearly suitable for Ne thermochronometry and cosmogenic ^{21}Ne observations. However, in most cases olivine and pyroxene may be insufficiently rich in U and Th to contain enough nucleogenic ^{21}Ne for accurate thermochronometry. For feldspars, on the other hand, our results suggest that exposure-dating using ^{21}Ne is most likely only possible under favorable conditions of temperature and grain size.

4.6. Retentivity of Ne at high temperatures

The kinetics of ^{21}Ne diffusion in both olivine and pyroxene suggest that cosmogenic ^{21}Ne in these minerals is not strongly susceptible to diffusive loss during subsequent reheating events such as proximal volcanic activity or other phenomena such as hydrothermal activity (Min and Reiners, 2007; Reiners et al., 2007; Shuster et al., 2010; Cooper et al., 2011). In Fig. 6 we show the duration and temperature curves (i.e., of constant Dt/a^2) that would result in 10% diffusive loss of previously-accumulated ^{21}Ne. Unless these minerals are heated to ~800 °C for durations of weeks to years, our results predict insignificant loss of previously accumulated ^{21}Ne. Conversely, brief reheating (<10 s) such as that associated with impact events (Shuster et al., 2010) will significantly disturb a cosmogenic ^{21}Ne concentration only if temperatures exceed 1100 °C.

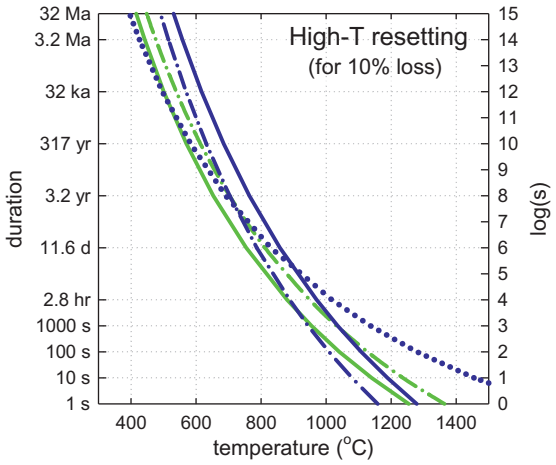

Fig. 6. Duration and temperature pairs that predict 10% diffusive loss of cosmogenic ^{21}Ne in olivine and pyroxene. Using our estimates of Ne diffusion kinetics calculated from sub-selected data (Table 1) and normalizing each to a diffusion domain radius of 500 μm, the curves correspond to values of Dt/a^2 associated with 10% diffusive loss. These curves indicate that significant quantities of cosmogenic ^{21}Ne will be retained in these minerals during heating events following exposure, such as forest fires or volcanic activity. The line style corresponding to the sample is the same as in Fig. 3.

4.7. Application to exposure-dating with ^{21}Ne in feldspars

Our observations for pyroxene and olivine predict that cosmogenic ^{21}Ne should without question be retained in these minerals over timescales relevant to surface exposure dating. As noted above, this is consistent with a number of exposure-dating studies that showed that (i) high temperatures are required to extract Ne from these minerals, and (ii) ^{21}Ne concentrations observed in these minerals are consistent with exposure ages inferred from other evidence. Our observations for feldspars, on the other hand, predict that cosmogenic ^{21}Ne is likely to be retained over exposure-dating timescales only in favorable circumstances. The only other evidence we are aware of that relates to this question consists of measurements of cosmogenic ^{21}Ne in coexisting quartz and sanidine from rhyolitic ignimbrites in Chile, with apparent exposure ages up to 4 Ma, by Kober et al. (2005). It is well established that cosmogenic ^{21}Ne is retained at Earth surface temperatures in quartz (e.g., Shuster and Farley, 2005), and Kober et al. (2005) observed that the ratios of cosmogenic ^{21}Ne in sanidine to that in quartz in five samples were approximately the same as the production ratios expected from the major element chemistry of the samples. They concluded that cosmogenic ^{21}Ne was most likely also quantitatively retained in sanidine at Earth surface temperatures.

Quantitative retention of cosmogenic ^{21}Ne in feldspars predicts that the ratio of cosmogenic ^{21}Ne in quartz to that in coexisting feldspar should always be equal to the production ratio, regardless of exposure age or geomorphic history. The ^{21}Ne production rate in quartz is reasonably well established (Amidon et al., 2009; Balco and Shuster, 2009; Goethals et al., 2009; Kober et al., 2011), but that

in feldspars is not. In addition, elemental production rates vary widely among rock-forming major elements, so the production rate in feldspar depends on its chemical composition. Because the ^{21}Ne production rate in quartz is fixed but that in feldspar varies with chemical composition, we have to normalize the feldspar/quartz ratios to a reference feldspar composition in order to compare them.

Kober et al. (2005) made a first-principles calculation of expected elemental production rates; although these overestimate (by ~10%) the observed ^{21}Ne production rate in quartz (because they were normalized to a production rate study that has been superseded by the references noted above), they can be used to estimate differences in production rates among samples with fairly similar chemical composition. We used these elemental production rates to compute model production rates for our feldspar samples as well as those of Kober et al. (2005), and applied these model production rates to normalize observed ^{21}Ne(feldspar)/^{21}Ne(quartz) ratios to a reference chemical composition (end-member anorthite; the only significance to the choice of anorthite is that its model production rate lies in the middle of the range predicted for possible feldspar compositions). (See Tables S3 and S4).

Fig. 7 shows that ^{21}Ne(feldspar)/^{21}Ne(quartz) ratios, when normalized to anorthite composition as we described, agree among all volcanic sanidine phenocrysts in this study and that of Kober et al. (2005); excluding one outlier (CN19 of Kober et al.), the mean normalized ^{21}Ne(feldspar)/^{21}Ne(quartz) ratio is 1.20 (reduced chi-square = 2.0 for 6 DOF; $p = 0.07$. The nominal error in the weighted mean is 0.04). This shows reasonable agreement with the model ratio of 1.12. There is no systematic relation between this ratio and the apparent exposure age of the sample (computed from the ^{21}Ne concentration in quartz; see Supplementary Table S2), which is strong evidence for quantitative retention of cosmogenic ^{21}Ne in volcanic sanidine phenocrysts over these durations. For comparison, using the Ne diffusion parameters estimated for FCs (Table 1), the calculation shown in Fig. 5 predicts only ~3% diffusive loss of cosmogenic ^{21}Ne from a 5 mm (radius) crystal during 500 kyr of accumulation at 20 °C. We conclude that cosmogenic ^{21}Ne is likely to be quantitatively retained in volcanic sanidine phenocrysts in most cases.

Further, these results provide a means of computing the cosmogenic ^{21}Ne production rate in sanidine; to compute a site- and sample-specific production rate, one should compute the ^{21}Ne production rate in quartz as described elsewhere, multiply by 1.20 ± 0.04 to obtain the production rate in end-member anorthite, and then apply a chemical composition factor derived from the model elemental production rates of Kober et al. (2005).

In contrast to the good agreement among samples and with expected production ratios observed for volcanic sanidine phenocrysts, alkali feldspars from the Antarctic granites display significantly lower concentrations of cosmogenic ^{21}Ne than coexisting quartz. In addition, the observed ratios are widely scattered. As the production rate of ^{21}Ne in alkali feldspar is expected to be higher than that in quartz, both of these observations indicate diffusive loss of cosmogenic ^{21}Ne. The observation that cosmogenic ^{21}Ne is quantitatively retained in volcanic sanidine phenocrysts, but not in granitic alkali feldspar, is not obviously consistent with our laboratory measurements of diffusion kinetics. The diffusion experiments indicate similar ^{21}Ne retention

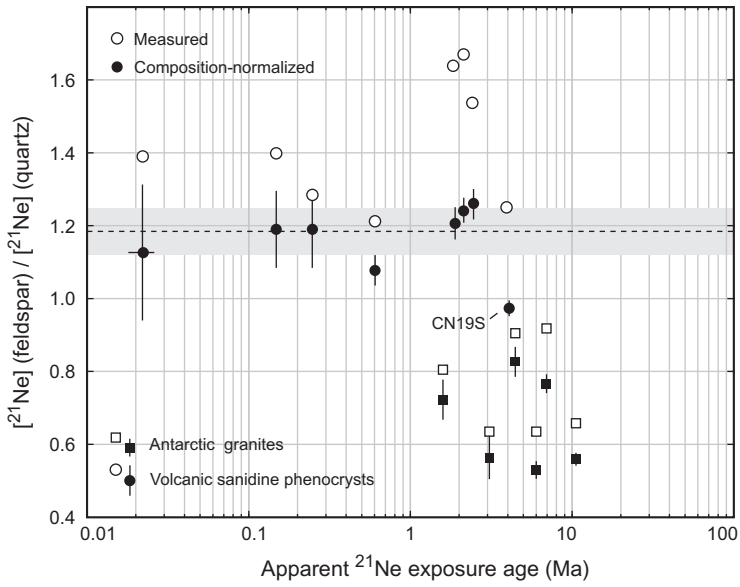

Fig. 7. Ratios of ^{21}Ne concentrations in coexisting feldspar and quartz. The open symbols show measured ratios; filled symbols show ratios corrected to a common chemical composition (end-member anorthite; see text and Supplementary Table S2). Measurements in volcanic sanidine phenocrysts from rhyolitic ignimbrites in this study and that of Kober et al. (2005) agree regardless of apparent exposure age, showing no evidence for ^{21}Ne loss. Measurements in alkali feldspars from Transantarctic Mountains granites, on the other hand, suggest significant diffusive loss of ^{21}Ne. The dashed line and gray band show the mean and standard deviation of anorthite-normalized ratios for ignimbrite measurements (excluding sample CN19S of Kober et al., 2005).

for sanidine and orthoclase (Fig. 3), and with slightly higher retentivity in orthoclase, not lower.

An important difference, however, is that we conducted our diffusion experiments on a sample of gem-quality orthoclase, whereas the alkali feldspars in the Antarctic granites display a perthitic exsolution texture, which is characteristic of most natural granitic alkali feldspar. It appears that un-exsolved feldspars (and probably strain-controlled perthites) may quantitatively retain cosmogenic ^{21}Ne under certain conditions, whereas granitic perthites with strain-free exsolution resulting from deuteric coarsening may not. In deuterically coarsened perthites, lamellar interfaces are incoherent, resulting in sub-grain domains (Parsons et al., 1999). Detailed analyses of Ar retention in granitic feldspars have shown that those with coherent strain-controlled exsolution (Parsons et al., 1999) retain Ar, whereas those with strain-free exsolution do not (McLaren et al., 2007; Harrison et al., 2010). This may simply reflect a reduction in the size of diffusion domains, or that the diffusivity of Ar in orthoclase from granites significantly differs from that in gem-quality feldspars. We conclude that ^{21}Ne retention in feldspars likely depends, in detail, on the composition and microtexture of the sample, but is unlikely in most granitic alkali feldspars. We hypothesize that the large volcanic phenocrysts shown in Fig. 7 may be acting as single diffusion domains and have therefore quantitatively retained cosmogenic ^{21}Ne. However, it appears that the granitic phenocrysts may have sub-grain domains that are smaller and limit their retentivity of ^{21}Ne, analogous to the multiple diffusion domain behavior of Ar in certain minerals (Lovera et al., 1991). Further work to quantify Ne diffusion kinetics among a broader range of compositions and textures may test this hypothesis.

5. CONCLUSION

Our results demonstrate the strong retentivity of Ne in olivine and pyroxene under experimental conditions and, by extension, at Earth surface temperatures. This shows, in agreement with other observations, that cosmogenic ^{21}Ne is quantitatively retained in these minerals at Earth surface conditions. Our experimentally-determined diffusion kinetics for feldspars, on the other hand, suggest that cosmogenic ^{21}Ne is only retained quantitatively in feldspars at Earth surface temperatures under favorable conditions of temperature, grain size, and mineral structure. This conclusion is consistent with our and others' observations that cosmogenic ^{21}Ne concentrations in naturally irradiated feldspars are sometimes, but not always, consistent with ^{21}Ne in coexisting, more retentive, minerals. Specifically, large phenocrysts of volcanic sanidine, which presumably act as a single diffusion domain, appear to quantitatively retain cosmogenic ^{21}Ne over timescales relevant to exposure-dating; however, granitic alkali feldspars with exsolution textures, that presumably act to reduce the size of diffusion domains, do not. Exposure dating with ^{21}Ne in feldspars will be quantitative in some favorable conditions, but may not be in others.

ACKNOWLEDGMENTS

The authors thank D. Cherniak, C. Gautheron, an anonymous reviewer, and P. Reiners for constructive comments. The authors acknowledge financial support from NSF Grant EAR-0738474 (to D.L.S.), the Ann and Gordon Getty Foundation. D.L.S. thanks M. Manga and L. Karlstrom for fruitful discussions which inspired some of these experiments. Mineral samples were provided by K. Righter and K. Farley, and samples of granite from Antarctica were provided by J. Stone.

APPENDIX A. SUPPLEMENTARY DATA

Supplementary data associated with this article can be found, in the online version, at http://dx.doi.org/10.1016/j.gca.2012.03.002.

REFERENCES

Albarède F. (2008) Rogue mantle helium and neon. *Science* **319**, 943–945.

Amidon W., Rood D. and Farley K. (2009) Cosmogenic ^{3}He and ^{21}Ne production rates calibrated against ^{10}Be in minerals from the Coso volcanic field. *Earth Planet. Sci. Lett.* **280**, 194–204.

Bachmann O., Dungan M. A. and Lipman P. W. (2002) The Fish Canyon magma body, San Juan volcanic field, Colorado: rejuvenation and eruption of an upper-crustal batholith. *J. Petrol.* **43**, 1469–1503.

Balco G. and Shuster D. L. (2009) Production rate of cosmogenic ^{21}Ne in quartz estimated from ^{10}Be, ^{26}Al, and ^{21}Ne concentrations in slowly eroding Antarctic bedrock surfaces. *Earth Planet. Sci. Lett.* **281**, 48–58.

Basu S., Murty S. V. S. and Kumar A. (2005) U, Th–21Ne, a new dating tool: a case study of apatites from Hogenakal carbonatites. *Curr. Sci.* **88**, 445–448.

Baxter E. F. (2010) Diffusion of noble gases in minerals. *Rev. Mineral. Geochem.* **72**, 509–557.

Blard P.-H., Puchol N. and Farley K. A. (2008) Constraints on the loss of matrix-sited helium during vacuum crushing of mafic phenocrysts. *Geochim. Cosmochim. Acta* **72**, 3788–3803.

Bromley G. R. M., Hall B. L., Stone J. O., Conway H. and Todd C. E. (2010) Late Cenozoic deposits at Reedy Glacier, Transantarctic Mountains: implications for former thickness of the West Antarctic Ice Sheet. *Quat. Sci. Rev.* **34**, 384–398.

Broxton D. E., Warren R. G., Byers F. M. and Scott R. B. (1989) Chemical and mineralogical trends within the Timber Mountain-Oasis Valley caldera complex, Nevada: evidence for multiple cycles of chemical evolution in a long-lived silicic magma system. *J. Geophys. Res.* **94**, 5961–5985.

Bruno L. A., Baur H., Graf T., Schlüchter C. H., Signer P. and Wieler R. (1997) Dating of Sirius Group tillites in the Antarctic Dry Valleys with cosmogenic ^{3}He and ^{21}Ne. *Earth Planet. Sci. Lett.* **147**, 37–54.

Cassata W. S. (2011) An isochron approach to ^{21}Ne cosmic ray exposure dating by activation with deuteron–deuteron fusion neutrons. *Chem. Geol.* **284**, 21–25.

Cassata W. S., Renne P. R. and Shuster D. L. (2009) Argon diffusion in plagioclase and implications for thermochronometry: a case study from the Bushveld Complex, South Africa. *Geochim. Cosmochim. Acta* **73**, 6600–6612.

Cassata W. S., Renne P. R. and Shuster D. L. (2011) Argon diffusion in pyroxenes: implications for thermochronometry and mantle degassing. *Earth Planet. Sci. Lett.* **304**, 407–416.

Cherniak D. J. and Watson E. B. (2011) Helium diffusion in rutile and titanite, and consideration of the origin and implications of diffusional anisotropy. *Chem. Geol.* **288**, 149–161.

Christiansen R.L. and Lipman P.W. (1965) Geologic map of the Topopah Springs NW quadrangle Nye County, Nevada, *U.S. Geological Survey Geologic Quadrangle Map* GQ-444, scale 1:24,000.

Christiansen R. L., Lipman P. W., Carr W. J., Byers, Jr., F. M., Orkild P. P. and Sargent K. A. (1977) Timber Mountain-Oasis Valley caldera complex of southern Nevada. *Geol. Soc. Am. Bull.* **88**, 943–959.

Cooper F. J., van Soest M. C. and Hodges K. V. (2011) Detrital zircon and apatite (U–Th)/He geochronology of intercalated baked sediments: a new approach to dating young basalt flows. *Geochem. Geophys. Geosyst.* **12**, Q07003. http://dx.doi.org/10.1029/2011GC003650.

Dowty E. (1980) Crystal-chemical factors affecting the mobility of ions in minerals. *Am. Min.* **65**, 174–182.

Eberhardt P., Eugster O. and Marti K. (1965) A redetermination of the isotopic composition of atmospheric neon. *Z. Naturforsch. A: J. Phys. Sci.* **20a**, 623–624.

Fechtig H. and Kalbitzer S. (1966) The diffusion of argon in potassium-bearing solids. In *Potassium-Argon Dating* (eds. O. A. Shaeffer, J. Zähringer). Springer-Verlag, Berlin, New York, pp. 68–106.

Fenton C. R., Niedermann S., Goethals M. M., Scheinder B. and Wijbrans J. (2009) Evaluation of cosmogenic ^{3}He and ^{21}Ne production rates in olivine and pyroxene from two Pleistocene basalt flows, western Grand Canyon, AZ, USA. *Quat. Geochronol.* **4**, 475–492.

Fernandez-Mosquera D., Hahm D. and Marti K. (2010) Calculated rates of cosmic ray muon-produced Ne in subsurface quartz. *Geophys. Res. Lett.* **37**. http://dx.doi.org/10.1029/2010GL044106.

Fortier S. M. and Giletti B. J. (1989) An empirical model for predicting diffusion coefficients in silicate minerals. *Science* **245**, 1481–1484.

Futagami T., Ozima S., Nagai S. and Aoki Y. (1993) Experiments on thermal release of implanted noble gases from minerals and their implications for noble gases in lunar soil grains. *Geochim. Cosmochim. Acta* **57**, 3177–3194.

Gautheron C. E., Tassan-Got L. and Farlay K. A. (2006) (U–Th)/Ne chronometry. *Earth Planet. Sci. Lett.* **243**, 520–535.

Goethals M., Hetzel R., Niedermann S., Wittmann H., Fenton C. R., Kubik P. W., Christl M. and von Blanckenburg F. (2009) An improved experimental determination of cosmogenic ^{20}Be/^{21}Ne and ^{26}Al/^{21}Ne production ratios in quartz. *Earth Planet. Sci. Lett.* **284**, 187–198.

Harrison T. M., Heizler M. T., McKeegan K. D. and Schmitt A. K. (2010) In situ ^{40}K–^{40}Ca "double-plus" SIMS dating resolves Klokken feldspar ^{40}K–^{40}Ar paradox. *Earth Planet. Sci. Lett.* **299**, 426–433.

Hart S. R. (1984) He diffusion in olivine. *Earth Planet. Sci. Lett.* **70**, 297–302.

Ivy-Ochs S., Kober F., Alfimov V., Kubik P. W. and Synal H.-A. (2007) Cosmogenic Be-10, Ne-21, and Cl-36 in sanidine and quartz from Chilean ignimbrites. *Nucl. Instrum. Methods Phys. Res. B* **259**, 588–594.

Kober F., Ivy-Ochs S., Leya I., Baur H., Magna T., Wieler R. and Kubik P. W. (2005) In situ cosmogenic Be-10 and Ne-21 in sanidine and in situ cosmogenic He-3 in Fe-Ti-oxide minerals. *Earth Planet. Sci. Lett.* **236**, 404–418.

Kober F., Ivy-Ochs S., Schlunegger F., Baur H., Kubik P. W. and Wieler R. (2007) Denudation rates and a topography-driven rainfall threshold in northern Chile: multiple cosmogenic nuclide data and sediment yield budgets. *Geomorphology* **83**, 97–120.

Kober F., Alfimov V., Ivy-Ochs S., Kubik P. W. and Wieler R. (2011) The cosmogenic ^{21}Ne production rate in quartz evaluated on a large set of existing ^{21}Ne–^{10}Be data. *Earth Planet. Sci. Lett.* **302**, 163–171.

Lemelle L., Guyot F., Leroux H. and Libourel Gu (2001) An experimental study of the external reduction of olivine single crystals. *Am. Mineral.* **86**, 47–54.

Leya I., Busemann H., Baur H., Wieler R., Gloris M., Neumann S., Michel R., Sudbrock F. and Herpers U. (1998) Cross sections for the proton-induced production of He and Ne isotopes from magnesium, aluminum, and silicon. *Nucl. Instrum. Methods Phys. Res. Sect. B: Beam Interact. Mater. At.* **145**, 449–458.

Lippolt H. J. and Weigel E. (1988) ^{4}He diffusion in ^{40}Ar rententive minerals. *Geochim. Cosmochim. Acta* **52**, 1449–1458.

Lovera O. M., Richter F. M. and Harrison T. M. (1991) Diffusion domains determined by ^{39}Ar release during step heating. *J. Geophys. Res.* **96**, 2057–2069.

McLaren S., Dunlap W. J. and Powell R. (2007) Understanding K-feldspar ^{40}Ar/^{39}Ar data: reconciling models, methods and microtextures. *J. Geol. Soc.* **164**, 941–944.

Mills, Jr., J. G., Saltoun B. W. and Vogel T. A. (1997) Magma batches in the Timber Mountain magmatic system, Southwestern Nevada Volcanic Field, Nevada, USA. *J. Volcanol. Geoth. Res.* **78**, 185–208.

Min K. and Reiners P. W. (2007) High temperature Mars-to-Earth transfer of meteorite ALH84001. *Earth Planet. Sci. Lett.* **260**, 72–85.

Minor S. A., Sawyer D. A., Wahl R. R., Frizzell, Jr., V. A., Schilling S. P., Warren R. G., Orkild P. P., Coe J. A., Hudson M. R., Fleck R. J., Lanphere M. A., Swadley W. C. and Cole J. C. (1993) *Preliminary Geologic Map of the Pahute Mesa 30′ × 60′ Quadrangle, Nevada*. U.S. Geological Survey Open-File Report, pp. 93–299.

Niedermann S. (2002) Cosmic-ray-produced noble gases in terrestrial rocks: dating tools for surface processes. In *Noble Gases in Geochemistry and Cosmochemistry* (eds. D. Porcelli, C. J. Ballentine, R. Wieler). Reviews in Mineralogy and Geochemistry, vol. 47. Mineralogical Society of America, pp. 731–784.

Niedermann S., Graf T. and Marti K. (1993) Mass spectrometric identification of cosmic-ray-produced neon in terrestrial rocks with multiple neon components. *Earth Planet. Sci. Lett.* **118**, 65–73.

Niedermann S., Graf T., Kim J. S., Kohl C. P., Marti K. and Nishizumi K. (1994) Cosmic-ray-produced 21Ne in terrestrial quartz: the neon inventory of Sierra Nevada quartz separates. *Earth Planet. Sci. Lett.* **125**, 341–355.

Parsons I., Brown W. L. and Smith J. V. (1999) ^{40}Ar/^{39}Ar thermochronology using alkali feldspars: real thermal history or mathematical mirage of microtexture? *Contrib. Mineral. Petrol.* **136**, 92–110.

Phillips W. M., McDonald E. V., Reneau S. L. and Poths J. (1998) Dating soils and alluvium with cosmogenic 21Ne profiles: case studies from the Pajarito Plateau, New Mexico, USA. *Earth Planet. Sci. Lett.* **160**, 209–223.

Poreda R. J. and Cerling T. E. (1992) Cosmogenic neon in recent lavas from the western United States. *Geophys. Res. Lett.* **19**, 1863–1866.

Porcelli D., Ballentine C. J. and Wieler R. (2002) An overview of noble gas geochemistry and cosmochemistry. *Rev. Mineral. Geochem.* **47**, 1–19.

Reiners P. W., Thomson S. N., McPhillips D., Donelick R. A. and Roering J. J. (2007) Wildfire thermochronology and the fate and transport of apatite in hillslope and fluvial environments. *J. Geophys. Res.* **112**, F04001. http://dx.doi.org/10.1029/2007JF000759.

Righter K. R. and Carmichael I. S. E. (1993) Mega-xenocrysts in alkali olivine basalts: fragments of disrupted mantle assemblages. *Am. Mineral.* **78**, 1230–1245.

Sawyer D. A., Fleck R. J., Lanphere M. A., Warren R. G., Broxton D. E. and Hudson M. R. (1994) Episodic caldera volcanism in the Miocene southwestern Nevada Volcanic field: revised stratigraphic framework, $^{40}Ar/^{39}Ar$ geochronology, and implications for magmatism and extension. *Geol. Soc. Am. Bull.* **106**, 1304–1318.

Schäfer J. M., Ivy-Ochs S., Wieler R., Leya I., Baur H., Denton G. H. and Schlüchter C. (1999) Cosmogenic noble gas studies in the oldest landscape on earth: surface exposure ages of the Dry Valleys, Antarctica. *Earth Planet. Sci. Lett.* **167**, 215–226.

Schäfer J. M., Baur H., Denton G. H., Ivy-Ochs S., Marchant D. R., Schlüchter C. and Wieler R. (2000) The oldest ice on Earth in Beacon Valley, Antarctica: newa evidence from surface exposure dating. *Earth Planet. Sci. Lett.* **179**, 91–99.

Shuster D. L. and Farley K. R. (2004) Diffusion kinetics of proton-induced ^{21}Ne, ^{3}He and ^{4}He in Quartz. *Geochim. Cosmochim. Acta* **69**, 2349–2359.

Shuster D. L. and Farley K. A. (2005) $^{4}He/^{3}He$ thermochronometry: theory, practice, and potential complications. *Rev. Mineral. Geochem.* **45**, 181–203.

Shuster D. L. and Farley K. A. (2009) The influence of artificial radiation damage and thermal annealing on helium diffusion kinetics in apatite. *Geochim. Cosmochim. Acta* **73**, 183–196.

Shuster D. L., Farley K. A., Sisterton J. M. and Burnett D. S. (2004) Quantifying the diffusion kinetics and spatial distributions of radiogenic ^{4}He in minerals containing proton-induced ^{3}He. *Earth Planet. Sci. Lett.* **217**, 19–32.

Shuster D. L., Balco G., Cassata W. S., Fernandes Vera A., Garrick-Bethell I. and Weiss B. (2010) A record of impacts preserved in the lunar regolith. *Earth Planet. Sci. Lett.* **290**, 155–165.

Thomas J.-B., Cherniak D. L. and Watson E. B. (2008) Lattice diffusion and solubility of argon in forsterite, enstatite, quartz, and corundum. *Chem. Geol.* **253**, 1–22.

Tolstikhin I., Kamensky I., Tarakanov S., Kramers J., Pekala M., Skiba V., Gannibal M. and Novikov D. (2010) Noble gas isotope sites and mobility in mafic rocks and olivine. *Geochim. Cosmochim. Acta* **74**, 1436–1447.

Trull T. W. and Kurz M. D. (1993) Experimental measurements of ^{3}He and ^{4}He mobility in olivine and clinopyroxene at magmatic temperatures. *Geochim. Cosmochim. Acta* **57**, 1313–1324.

Trull T. W., Kurz M. D. and Jenkins W. J. (1991) Diffusion of cosmogenic ^{3}He in olivine and quartz: implications for surface exposure dating. *Earth Planet. Sci. Lett.* **103**, 241–256.

Vogel T. A. and Aines R. (1996) Melt inclusions from chemically zoned ash flow sheets from the Southwest Nevada Volcanic Field. *J. Geophys. Res.* **101**, 5591–5610.

Warren G. R., Byers F. M., Broxton D. E., Freeman S. H. and Hagan R. C. (1989) Phenocryst abundance and glass and phenocryst compositions as indicators of magmatic environments of large-volume ash flow sheets in southwestern Nevada. *J. Geophys. Res.* **94**, 5987–6020.

Wartho J.-A., Kelley S. P., Brooker R. A., Caroll M. R., Villa I. M. and Lee M. R. (1999) Direct measurement of Ar diffusion profiles in a gem-quality Madagascar K-feldspar using the ultra-violet laser ablation microprobe (UVLAMP). *Earth Planet. Sci. Lett.* **170**, 141–153.

Wolf R. A., Farley K. A. and Kass D. M. (1998) Modeling of temperature sensitivity of the apatite (U–Th)/He thermochronometer. *Chem. Geol.* **148**, 105–114.

Zhao Z.-F. and Zheng Y.-F. (2007) Diffusion compensation for argon, hydrogen, lead, and strontium in minerals: empirical relationships to crystal chemistry. *Am. Mineral.* **92**, 289–308.

Associate editor: Peter Reiners